

A 30nA Quiescent 80nW to 14mW Power Range Shock-Optimized SECE-based Piezoelectric Harvesting Interface with 420% Harvested Energy Improvement

Anthony Quelen, Adrien Morel, Pierre Gasnier, Romain Grézaud, Stéphane Monfray, Gaël Pillonnet

Univ. Grenoble Alpes, CEA, LETI, MINATEC, F-38000 Grenoble, France.
STMicroelectronics, Grenoble, France.

Piezoelectric Energy Harvesters (PEH) are usually used to convert mechanical energy (vibration, shocks) into electrical energy, in order to supply energy-autonomous sensor nodes in industrial, biomedical or domotic applications. Non-linear extraction strategies such as Synchronous Electrical Charge Extraction (SECE) [1-2], energy investing [3] or Synchronized Switch Harvesting on Inductor (SSHI) [4] have been developed to maximize the extracted energy from harmonic excitations. However, in most of today's applications, vibrations are not periodic and mechanical shocks occur at unpredictable rates [4]. SSHI interfaces naturally seemed to be the most appropriate candidate for harvesting shocks as they exhibit outstanding performance in periodic excitations [4]. However, the SSHI strategy presents inherent weaknesses while harvesting shocks, since the invested energy stored in the piezoelectric capacitance cannot be recovered.

In this work, we propose a self-starting, battery-less, 0.55mm² integrated energy harvesting interface based on SECE strategy which has been optimized to work under shock stimulus. Due to the sporadic nature of mechanical shocks which imply long periods of inactivity and brief energy peaks, the interface's average consumption is optimized by minimizing the quiescent power. A dedicated energy saving sequencing has thus been designed, reducing the static current to 30nA and enabling energy to be extracted with only one single 8μJ shock occurring every 100s. Our SECE-based circuit features a shock FoM 1.6x greater than previous SSHI-based interfaces [4].

The proposed system depicted in Fig.1 is made of a negative voltage converter rectifying the PEH output voltage, and a SECE power path controlled by a sequenced circuit. The sequencing is divided in 4 phases and the associated time diagrams are illustrated in Fig.2. During the sleeping mode T_1 , all blocks except the shock detection (SD) are turned off. During the starting phase, the energy is stored in C_{ASIC} through a cold-start path, increasing V_{ASIC} . This will progressively turn on the SD. Next, when stress applied to the piezoelectric material leads to an increase in V_{REC} , the SD checks if the electrical energy

converted by the piezoelectric transducer is sufficiently high to be harvested ($V_{REC} > V_{ASIC}$). By setting $Flag_{SHOCK}$, the SD enables the V_{ASIC} detection which determines whether the cold start path should be activated. If V_{ASIC} is below 1.5V, we consider that the stored energy is insufficient to start the SECE operation, and the cold start path remains connected in order to keep on charging C_{ASIC} . If this is not the case, the detection block sends the $Flag_{START}$ signal which disables the cold start, enables the peak detection and starts the maximum voltage detection phase T_2 . When V_{REC} reaches its maximum, the system enters its harvesting phase T_3 . V_{N1} is set high, which connects the inductance L with the piezoelectric capacitance, C_P . The dual mode comparator (DMC) is used in its zero crossing detection (ZCD) configuration, and detects when V_{REC} goes below $V_{TL} = -14mV$, which means that almost all the energy previously stored in C_P has been extracted in L . Then, the system starts its storing phase T_4 . N_1 is turned off, while P_2 and N_2 are turned on. The instant I_L reaches zero, which is detected by the same DMC used in its Reverse Current Detection (RCD) configuration, indicates that all the energy that was stored in L during T_3 has been transferred in C_{STORE} . Ultimately, the system returns to its sleep mode T_1 , waiting the next energy event. N_3 acts as a freewheeling diode and provides a path to dissipate the remaining energy in L .

Fig.3 shows detailed transistor-level schematics of the DMC and the Shock and V_{ASIC} Detections. During T_3 , the DMC is enabled in its ZCD configuration. M_2 and M_4 constitute a differential pair allowing V_{REC} to be compared with the ground voltage. Due to M_1 , when V_{REC} is high, only $\frac{1}{4}$ of the bias current flows through M_1 and M_2 . As V_{REC} decreases (thanks to the charge transfer occurring between C_P and L), the current in M_2 is increased, which improves the detection accuracy. Furthermore, the circuit consumption is reduced when V_{REC} is high, since it is only useful to increase the comparator performances when V_{REC} gets close to 0V. V_{HYST} is initially high, which creates a -14mV offset on the input of the comparator. The circuit also includes a comparator which is used to accurately implement the zero crossing detection. During T_4 , the DMC switches to its RCD configuration. V_{HYST} is set low, which suppresses the -14mV offset. In this phase, V_{REC} is proportional to $-I_L$, as N_2 is turned on. Therefore, when I_L decreases, V_{REC} increases until it reaches 0V. Then, T_1 starts. The DCM is disabled in order to avoid any unnecessary energy consumption, and only the SD is powered. Therefore, during T_1 , the $30nA@1.5V$ current drawn from C_{ASIC} is the one flowing through M_{17} , as shown in Fig.3. When V_{REC} increases, current starts flowing through M_{14} which forces M_{16} 's drain potential to increase. If $V_{REC} > V_{ASIC}$, then $Flag_{Shock}$ becomes high, which consequently enables the V_{ASIC} Detector by forcing M_{20} conduction. To avoid any ringing, a resistance R_{HYS} is used to create a difference between the

high (1.5V) and low (1.4V) threshold. The integrated resistances R_1 and R_2 enable the minimum of V_{ASIC} to be selected, to ensure the self-operation of the chip. In our case, we fixed this minimum V_{ASIC} at 1.5V. When this condition is satisfied, $Flag_{Start}$ is set high, thanks to a two-stage comparator.

Our chip was fabricated in CMOS 40nm technology including 10V devices, and occupies a 0.55mm^2 core area (Fig.7). In order to emulate both periodic and shock excitations, a MIDE piezoelectric generator (PPA1011) with a 5.67g mobile mass and a resonant frequency of 75.4 Hz has been placed on a shaker. The harvester has an intrinsic capacitance C_P of 43nF. Fig.4 shows multiscale experimental waveforms of the interface circuit undergoing shocks with C_{STORE} and C_{ASIC} initially discharged. The shocks are applied every second, with various accelerations from 5 to 16G. The off-chip inductance L and capacitances C_{STORE} and C_{ASIC} values are 2.2mH, 100 μ F, and 10 μ F, respectively. After the first three shocks, which are used to store enough energy in C_{ASIC} thanks to the cold start power path, the system operates autonomously in its optimized mode and the energy is stored in C_{STORE} . For test purposes, when V_{STORE} reaches 2.8V, the energy monitoring block intermittently connects a 1k Ω load resistance to emulate the consumption of a sensor.

The power stored in C_{STORE} was measured under shock and periodic vibrations for many V_{STORE} as shown in Fig.5. From weak to strong shocks, our chip harvested 2.8x to 4.2x more than the maximal energy harvested using an on-chip full bridge rectifier interface, while it reached a FoM of 3.14 under periodic excitation. In Fig.6, the performance of our chip is compared to prior art. We obtained a 1.6x shock FoM enhancement in comparison to previous work [4]. Our system also shows the best FoM under periodic excitation compared to other SECE interfaces [1-2]. The measured maximum end-to-end efficiency of our circuit is 94% under periodic excitation at 82 μ W which is the highest end-to-end efficiency compared to former work [1-4]. The measured quiescent current in sleeping mode is 30nA@1.5V. This allows self-operation of our circuit with an input power as low as 80nW. We were able (using various PEH) to maintain an efficiency over 70% for input power below 14mW. The proposed IC in 40nm technology allows to add harvesting functionalities within a microcontroller die.

References:

- [1] P. Gasnier *et al.*, "An Autonomous Piezoelectric Energy Harvesting IC Based on a Synchronous Multi-Shot Technique," *IEEE Journal of Solid-State Circuits*, vol. 49, no. 7, pp. 1561–1570, 2014.
- [2] T. Hehn *et al.*, "A Fully Autonomous Integrated Interface Circuit for Piezoelectric Harvesters," *IEEE Journal of Solid-State Circuits*, vol. 47, no. 9, pp. 2185–2198, 2012.
- [3] D. Kwon *et al.*, "A single-inductor 0.35- μm CMOS energy-investing piezoelectric harvester," *IEEE International Solid-State Circuits Conference*, pp. 78–79, 2013.
- [4] D. A. Sanchez *et al.*, "21.2 A 4 μW -to-1mW parallel-SSHI rectifier for piezoelectric energy harvesting of periodic and shock excitations with inductor sharing, cold start-up and up to 681% power extraction improvement," *IEEE International Solid-State Circuits Conference*, pp. 366–367, 2016.

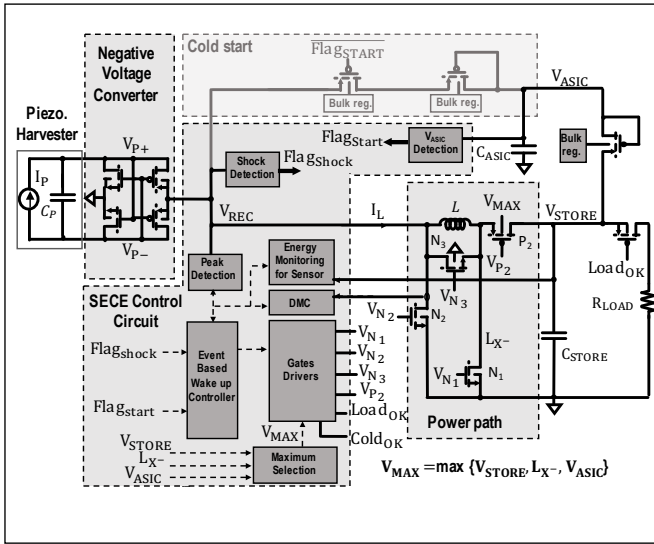


Figure 1: Piezoelectric interface overview.

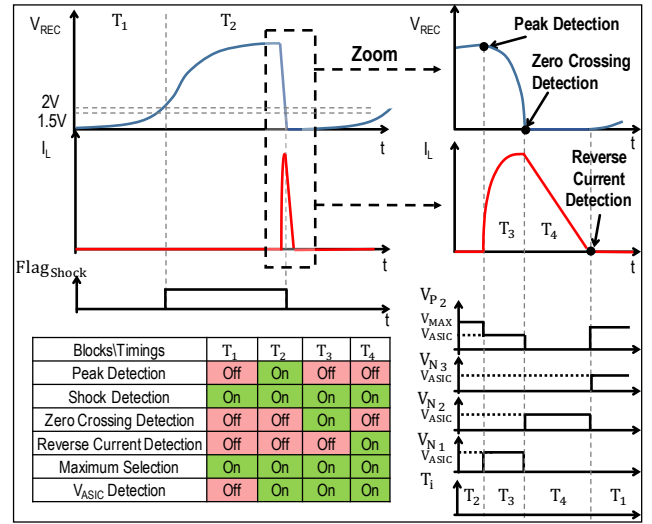


Figure 2: Waveforms, chronograms and sequencing of the control circuit.

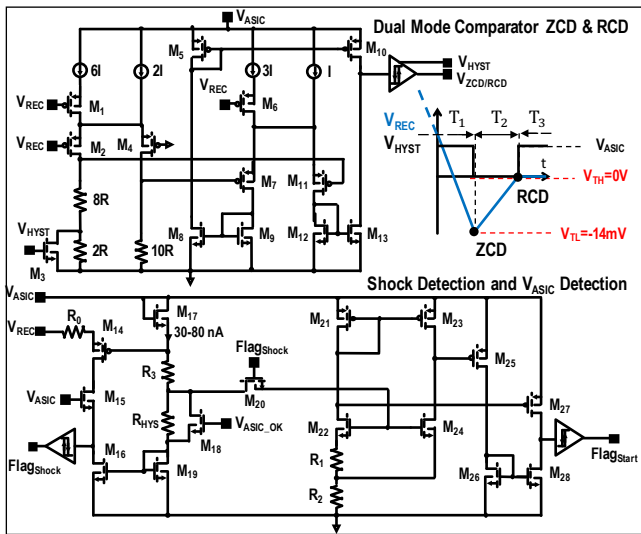


Figure 3: Dual mode comparator and shock detector schematics

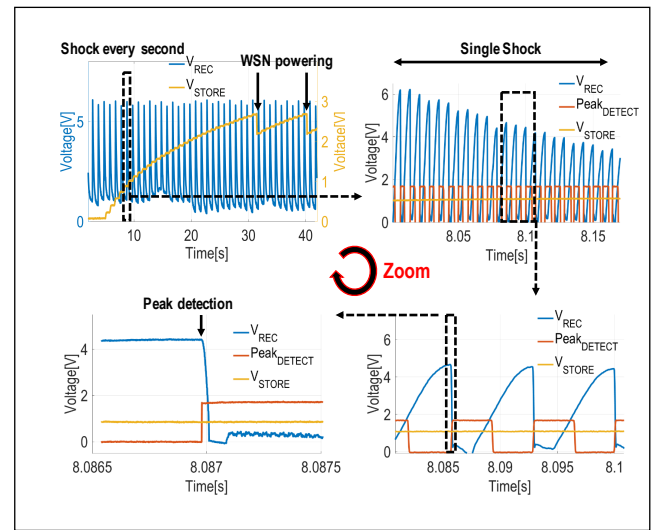


Figure 4: Measured transient waveforms of the proposed interface.

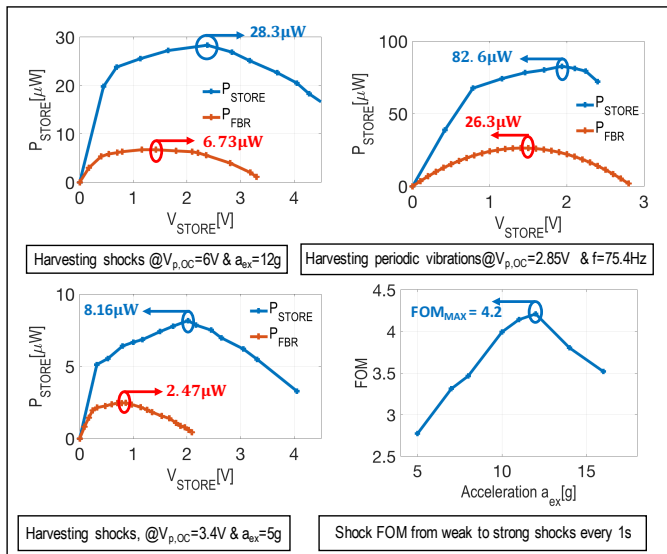


Figure 5: Measured harvested power comparison between our interface and using an active standalone full bridge rectifier (FBR).

	[1]	[2]	[3]	[4]	This Work	Unit
Technology	350	350	350	350	40	nm
Chip Size	3.6	1.25	2.34	0.72	0.55	mm ²
Scheme Type	SECE	SECE	Energy Investing	SSHI	SECE	-
Piezoelectric Harvester	Murata	MIDE V22B	MIDE V22B	MIDE V21B & V22B	MIDE PPA1011	-
C _p	23	19.5	15	26	43	nF
Excitation type	Periodic	Periodic	Periodic & Shock	Periodic & Shock	Periodic & Shock	-
Operation Frequency	100	174	143	225	75.4	Hz
FOM (periodic) ⁽²⁾	≈ 170 ⁽¹⁾	206	360	681	314	%
FOM (shocks) ⁽³⁾	N/A	N/A	-	269	420	%
Cold Startup	Yes	Yes	No	Yes	Yes	-
End-to-end Efficiency	61	85.3	69.2	≈ 88 ⁽¹⁾	94	%
Input power range	10-1000	5-500	-	4-1000	0.080-14000	μW
Quiescent current	1	0.3	0.1	≈ 1 ⁽¹⁾	0.03	μA

(1) Calculated from the paper (2) FOM (periodic) = $\frac{\max(P_{out})}{F \cdot V_{oc}^2 \cdot C_p}$ (3) FOM (shocks) = $\frac{\max(P_{out})}{\max(P_{out, FBR})}$

Figure 6: Performances comparison with prior art.